Decoherence of matter waves by thermal emission of radiation

Lucia Hackermüller, Klaus Hornberger, Björn Brezger*, Anton Zeilinger & Markus Arndt

[1]*Institut für Experimentalphysik, Universität Wien, Boltzmanngasse 5, A-1090 Wien, Austria*

* Present address: Fachbereich Physik, Universität Konstanz, D-78457 Konstanz, Germany

Emergent quantum technologies have led to increasing interest in decoherence—the processes that limit the appearance of quantum effects and turn them into classical phenomena. One important cause of decoherence is the interaction of a quantum system with its environment, which 'entangles' the two and distributes the quantum coherence over so many degrees of freedom as to render it unobservable. Decoherence theory[1–4] has been complemented by experiments using matter waves coupled to external photons[5–7] or molecules[8], and by investigations using coherent photon states[9], trapped ions[10] and electron interferometers[11,12]. Large molecules are particularly suitable for the investigation of the quantum–classical transition because they can store much energy in numerous internal degrees of freedom; the internal energy can be converted into thermal radiation and thus induce decoherence. Here we report matter wave interferometer experiments in which C_{70} molecules lose their quantum behaviour by thermal emission of radiation. We find good quantitative agreement between our experimental observations and microscopic decoherence theory. Decoherence by emission of thermal radiation is a general mechanism that should be relevant to all macroscopic bodies.

In this Letter we investigate the decoherence of molecular matter waves. We change the internal temperature of the molecules in a controlled way before they enter a near-field interferometer, and observe the corresponding reduction of the interference contrast. The idea behind this effort is to demonstrate a most fundamental decoherence mechanism that we encounter in the macroscopic world: all large objects, but also molecules of sufficient complexity, are able to store energy and to interact with their environment via thermal emission of photons. It is generally believed that warm macroscopic bodies emit far too many photons to allow the observation of de Broglie interferences, whereas individual atoms or molecules can be sufficiently well isolated to exhibit their quantum nature. However, there must be a transition region between these two limiting cases. Interestingly, as we show in this study, C_{70} fullerene molecules have just the right amount of complexity to exhibit perfect quantum interference in our experiments[13] at temperatures below 1,000 K, and to gradually lose all their quantum behaviour when the internal temperature is increased up to 3,000 K. We can thus trace the quantum-to-classical transition in a controlled and quantitative way. The complexity of large molecules adds a novel quality with respect to previously performed experiments with atoms[5–7]: the energy in molecules may be equilibrated in many internal degrees of freedom during the free flight, and a fraction of the vibrational energy will eventually be reconverted into emitted photons. Therefore the internal dynamics of the molecule is also relevant for the quantum behaviour of the centre-of-mass state. In contrast to resonance fluorescence, which was investigated with atoms[5–7], thermal decoherence is omnipresent in macroscopic systems and it cannot be switched off.

The basic set-up of our experiment[14] is sketched in Fig. 1: a beam of C_{70} molecules is generated by sublimation at about 900 K. The molecules pass a heating stage where they cross a focused argon ion laser beam up to 16 times. The fullerenes interact with the laser approximately every 0.3 mm. The laser heating increases the molecular temperature by 140 K per absorbed photon. We calculate that they reach up to 5,000 K for very short times, but the re-emission of thermal photons is so efficient that even the hottest molecules are cooled to below ~3,000 K when they enter the interferometer 7.2 cm behind the heating stage.

The interferometer consists of three identical free-standing gold gratings with a period of $d = 991$ nm. They are separated by the equal distance of $L = 38$ cm, which is the Talbot length $L_T = d^2/\lambda_{dB}$ for a typical de Broglie wavelength of $\lambda_{dB} = 2.6$ pm. The first grating acts as a periodic array of narrow slit sources, the second one as the diffracting element, and the third grating is used as a scanning detection mask, which modulates the molecular density pattern produced by the Talbot–Lau interference effect[15,16]. The transmitted molecules are ionized by a blue laser beam (wavelength 488 nm, 6.6 μm waist), and their intensity I is recorded as a function of the lateral displacement of the third grating. The fringe visibility $V = (I_{max} - I_{min})/(I_{max} + I_{min})$ characterizes the interferogram and thereby the coherence of the molecular evolution.

The essence of the experiment is to measure the variation of the interference fringe visibility with heating laser power (Fig. 2). Two observations can be made: first, the interference contrast decreases

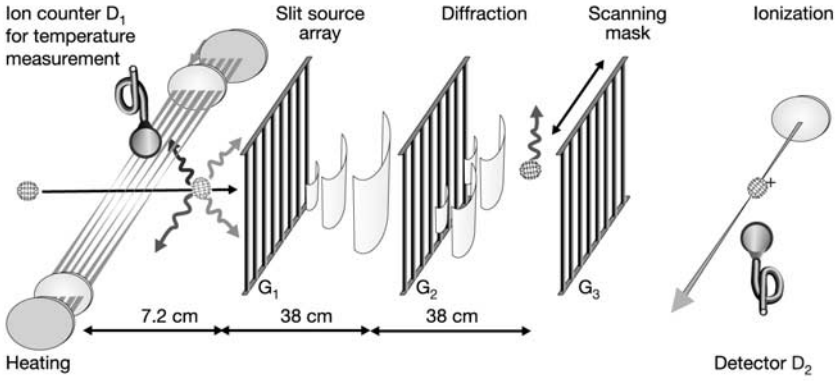

Figure 1 Set-up for the observation of thermal decoherence in a Talbot–Lau molecule interferometer. A fullerene beam passes from left to right, interacting with a heating stage, a three-grating (G_1–G_3) matter-wave interferometer and an ionizing detection laser beam in D_2 (wavelength 488 nm, $1/e^2$ intensity radius 6.6 μm, 15 W). The gold gratings have a period of 991 nm and slit widths of nominally 475 ± 20 nm. Decoherence of the fullerene matter waves can be induced by heating the molecules with multiple laser beams (514.5 nm, 40 μm waist radius, 0–10 W) before they enter the interferometer. The resulting molecular temperature can be assessed by detecting the heating-dependent fraction of fullerene ions using the electron multiplier D_1 over the heating stage.

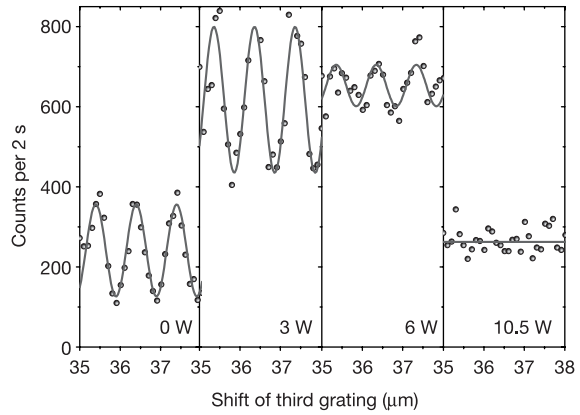

Figure 2 Molecule interferograms for C_{70} at 190 m s^{-1} for increasing laser heating powers, *P*. The fringe visibility *V* decreases with increasing heating power *P* owing to the rising emission probability of visible photons: $P = 0$ W ($V = 47\%$), $P = 3$ W ($V = 29\%$), $P = 6$ W ($V = 7\%$), $P = 10.5$ W ($V = 0\%$). In contrast to that, the absolute count rate grows initially with increasing *P*. This is due to the fact that the thermal ionization probability in detector D_2 increases with the temperature of the arriving molecules. At even higher heating intensities the count rate falls again because of ionization and fragmentation in the heating stage.

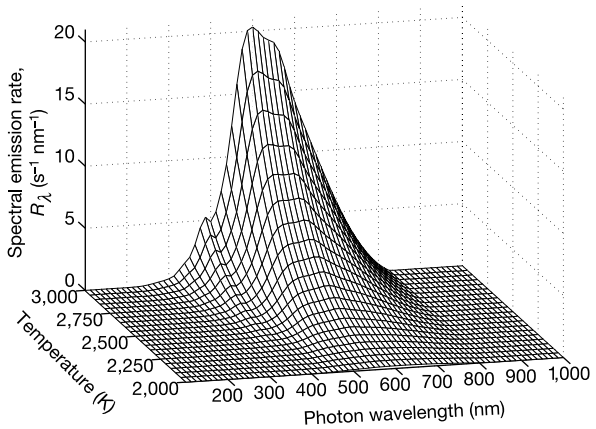

Figure 3 Spectral photon emission rate R_λ of C_{70} molecules, as used for the calculation of thermal decoherence. We use the published[25] absorption cross-section for ($S_0 \rightarrow S_1$) and a heat capacity of $C_V = 202\,k_B$. The fall-off to short wavelengths is determined by the limited internal energy of the molecules, while the decrease at long wavelengths is due to the lack of accessible radiative transitions at energies below ~1.5 eV. The figure shows that in the absence of cooling a single molecule at 2,500 K travelling at 190 m s^{-1} (that is, with a transit time of 4 ms through the interferometer) would emit an integrated number of three visible photons. This is sufficient to determine the path of the molecule if the emission occurs close to the second grating.

monotonically with increasing power, and vanishes at 10 W. This is the signature of decoherence due to the enhanced probability for the emission of thermal photons that carry 'which-path' information. Second, we notice that the count rate also varies considerably. This is explained by the dependence of the ionization efficiency in the detector D_2 on the internal energy of the fullerenes. It proves that much internal energy remains in the molecules during their flight through the apparatus.

In order to confirm quantitatively the interpretations of both observations, we model the evolution of the distribution of the internal energies on their way through the apparatus. The temperature dependence of the spectral photon emission rate (equation (1) below) then yields the loss of fringe visibility as predicted by decoherence theory (equation (2) below).

The first photon absorption populates the electronic triplet state T_1 via the excited singlet S_1. Given the known C_{70} triplet lifetimes and non-radiative transition rates (see ref. 17 and references therein), we can assume that all further excitation occurs in the triplet system and that the absorbed excess energy is rapidly transferred to the vibrational levels. It is known that fullerenes may store more than 100 eV for a very short time[17], and it was observed that at high temperatures three different cooling mechanisms start to compete—the thermal emission of photons, electrons or C_2 dimers[18–22]. These processes are the molecular analogues of the bulk phenomena known as blackbody radiation, thermionic emission and evaporative cooling. Following the most recent experimental data[22], we may safely assume that fragmentation is the least efficient mechanism. In contrast, thermally activated ionization is an important mechanism, which we use both in our fullerene detector[23] and for molecule thermometry, as discussed below. Nevertheless, we can safely neglect both delayed ionization and fragmentation for the discussion of the fringe contrast, because the recoil upon fragmentation and ionization is generally so large that the affected molecules will miss the narrow detector. We have also experimentally confirmed that neither C_{70}^+ ions nor C_{68} nor smaller fragments from the heating region are recorded by the detector D_2.

However, C_{70}^+ ions—and potentially ionized fragments—can be detected immediately above the heating stage by the electron multiplier D_1 (Fig. 1). To get an estimate of the molecular temperature distribution, we record the number of ions as a function of the heating power and of the fullerene velocity. By comparing the data with a model calculation, we can extract the parameters that govern the molecular heating of C_{70}. Our model describes the spatial and velocity-dependent distribution of the internal molecular energy by accounting for the stochastic absorption process, the laser beam characteristics, and the rapid radiative cooling between the beams as determined by equation (1) below. It reproduces the detected number of ions in the heating stage for different laser powers, different numbers of heating beams and all velocities with the fit parameters for the triplet absorption cross-section, $\sigma(T_1) = 2 \times 10^{-17}$ cm^2, and the effective Arrhenius constant for ionization, $A_{ion} = 5 \times 10^9$ s^{-1}. The same calculation also describes the heating-dependent increase in count rate at the detector D_2 and thus yields independent information on the temperature distribution in the molecular beam.

The mean temperature in the beam drops rapidly behind the heating stage through the emission of thermal photons. The emission of a continuous photon spectrum has already been observed for fullerenes in other experiments[18,24]. The equation for the thermal radiation density differs from the macroscopic Planck law for several reasons. First, the thermal wavelengths are much larger than the size of the fullerene, turning it into a coloured emitter. The mean emission probability is proportional to the usual mode density factor ω^2/π^2c^2 and the known frequency-dependent absorption cross-section[25] $\sigma_{abs}(\omega)$, assuming that it does not strongly depend on the internal temperature. Second, the particle is not in thermal equilibrium with the radiation field. It emits into a cold environment and stimulated emission does not occur. For this reason, the statistical factor $1/[\exp(\hbar\omega/k_BT) - 1)]$ of the Planck formula now would read $\exp(-\hbar\omega/k_BT)$. Third, the 204 vibrational modes of C_{70} do not constitute an infinite heat bath but have a finite heat capacity C_V. Therefore the emission does not take place at a fixed temperature, although the internal energy is nonetheless conveniently characterized by the micro-canonical temperature T_m. This leads to a further correction in the spectral photon emission rate[26], which is now fully described by

$$R_\omega(\omega, T_m) = \frac{\omega^2}{\pi^2 c^2}\sigma_{abs}(\omega)\exp\left[-\frac{\hbar\omega}{k_B T_m} - \frac{k_B}{2C_V}\left(\frac{\hbar\omega}{k_B T_m}\right)^2\right] \quad (1)$$

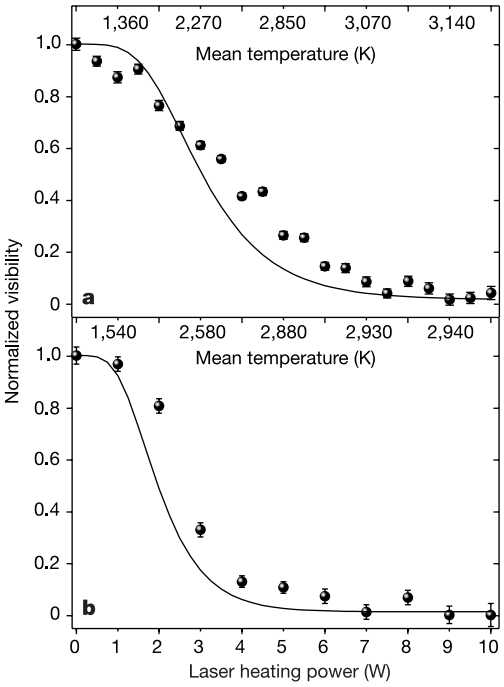

Figure 4 Decoherence curves. **a**, Interference visibility as a function of laser heating power (lower scale). The molecular beam with a mean velocity of $v_m = 190\,\mathrm{m\,s^{-1}}$ passes a 50 μm central height delimiter comparable to the waist (40 μm) of the 16 heating laser beams. We observe a rapid decrease of the fringe visibility with increasing power both in the experiment (circles) and in theory (solid line). The upper axis indicates the mean temperature of the molecules when they enter the interferometer. The maximum contrast without heating was $V_0 = 47\%$, which is close to the theoretical value[11]. **b**, Molecules with $v_m = 100\,\mathrm{m\,s^{-1}}$, selected by a 150 μm height delimiter and heated by ten beams of the specified incident laser power. The qualitative behaviour is the same and the quantitative agreement with theory is as good as before. The maximum contrast for this velocity class was $V_0 = 19\%$. In both experimental arrangements, a mean number between one and two visible photons is required to reduce the contrast by a factor of two.

In Fig. 3 we plot the wavelength dependence of $R_\lambda = R_\omega|\mathrm{d}\omega/\mathrm{d}\lambda|$. We observe that at temperatures below 2,000 K the emission rate is negligible, whereas at higher temperatures the molecules may emit photons whose wavelengths are comparable to (or even smaller than) the maximum path separation of ~1 μm. They transmit (partial) which-path information to the environment, leading to a reduced observability of the fullerene wave nature. Around 3,000 K the molecules have a high probability to emit several visible photons yielding sufficient which-path information to effect a complete loss of fringe visibility in our interferometer.

A formal description of this qualitative picture can be given by decoherence theory. It considers the entanglement of the molecule with the emitted photon, and shows how coherences vanish once a trace over the photon state is performed. For objects with velocity v and temperature evolution $T(t)$ we obtain a visibility

$$V = V_0 \exp\left[-\int_0^{2L/v} \mathrm{d}t \int_0^\infty \mathrm{d}\lambda\ R_\lambda(\lambda, T(t)) \times \left\{1 - \mathrm{sinc}\left(2\pi \frac{d}{\lambda} \cdot \frac{L - |vt - L|}{L_\mathrm{T}}\right)\right\}\right] \quad (2)$$

as discussed in the Methods section. V_0 denotes the interference contrast in the absence of photon emission. In the exponential, the sinc function compares the effective molecular path separation to the radiation wavelength, while the integrals cover all photon wavelengths λ and longitudinal positions vt in the interferometer. As a result, the visibility is reduced exponentially whenever photons are emitted whose wavelength is sufficiently small to resolve the path separation. Our predictions for the loss of visibility are obtained by weighting equation (2) with the previously determined distribution of temperature evolutions in the molecular beam.

In Fig. 4 we compare our decoherence model with the experiments by plotting the interference fringe visibility as a function of the laser power. We observe a strong decrease of the visibility for molecules at $190\,\mathrm{m\,s^{-1}}$, heated by 16 laser beams (Fig. 4a), and for molecules at $100\,\mathrm{m\,s^{-1}}$, heated by 10 laser beams (Fig. 4b).

We also observe good agreement between decoherence theory (solid line) and the experiment (circles). The experiment is reproducible within the indicated error bars for a given laser alignment, but small displacements of the laser focus will influence the shape and slope of the observed decoherence curve. The difference between the theoretical and the experimental curve is of the order of this variation.

In summary, we have presented conclusive empirical and numerical evidence for observation of the quantum-to-classical transition of a material object caused by its own emission of thermal radiation. This auto-localization is a fundamental process limiting the ultimate observability of quantum effects in macroscopic objects. However, for nanometre-sized systems[13,27,28] this mechanism becomes relevant only at high temperatures, and it is not expected to be a limitation for interference of objects even considerably larger than the fullerenes, such as proteins. □

Methods

Equation (2) describes the loss of matter wave coherence due to the emission of thermal photons. It is obtained by assuming that the emission is isotropic and that the absorbing walls of the apparatus are located in the far-field, where the photon position distribution reflects its momentum distribution. In this case, a trace over the photon state changes the fullerene centre-of-mass state $\hat{\rho}$ according to

$$\hat{\rho} \rightarrow \hat{\rho}' = \int \mathrm{d}\mathbf{k} \frac{p(k)}{4\pi k^2} \hat{U}_\mathbf{k} \hat{\rho} \hat{U}_\mathbf{k}^\dagger \quad (3)$$

where the $\hat{U}_\mathbf{k} = \exp(i\hat{\mathbf{r}}\mathbf{k})$ are momentum translation operators and $p(k)$ is the probability density for the photon wavenumber $k = 2\pi/\lambda$. In the position representation of the density matrix,

$$\rho'(\mathbf{r}_1, \mathbf{r}_2) \equiv \langle \mathbf{r}_1|\hat{\rho}'|\mathbf{r}_2\rangle = \langle \mathbf{r}_1|\hat{\rho}|\mathbf{r}_2\rangle \eta(\mathbf{r}_1 - \mathbf{r}_2) \quad (4)$$

we find from equation (3) that the off-diagonal elements are reduced by the decoherence function[29]

$$\eta(\mathbf{r}_1 - \mathbf{r}_2) = \frac{1}{R_\mathrm{tot}} \int_0^\infty \mathrm{d}\lambda\ R_\lambda(\lambda)\ \mathrm{sinc}\left(2\pi \frac{|\mathbf{r}_1 - \mathbf{r}_2|}{\lambda}\right) \quad (5)$$

Here $p(k)$ is expressed in terms of the spectral emission rate R_λ (see equation (1)) and the total photon emission rate R_tot. This sinc-shaped position dependence of η is also found in other experiments with isotropic momentum change[7,8]. It describes the diffraction limitation of a hypothetical microscope used to obtain which-path information on the molecules.

In the Talbot–Lau geometry[14,16,27] the final molecular fringe pattern $w(x)$ is strictly periodic in the grating constant d, and can be expanded as a Fourier series, which reads in the absence of decoherence

$$w(x) = \sum_l C_l \exp(2\pi i l x/d) \quad (6)$$

Assuming that a single photon emission occurs at the longitudinal position $z = vt$, a closed expression for the resulting molecular density pattern can be found. It is obtained by propagating the molecular density matrix in paraxial approximation first to the position z. We then apply the decohering transformation (equation (4)) followed by a propagation to the final grating. For a set-up with equally spaced and identical gratings, the new fringe pattern is described by a simple modification of the Fourier coefficients

$$C_l \rightarrow C_l' = C_l \cdot \eta(ld(L - |vt - L|)/L_\mathrm{T}) \quad (7)$$

In order to account for more than one photon emission, we make the Markov assumption that all photon emissions are independent of each other. Because the modification

(equation (7)) is independent of the molecular density matrix, the change of the final density pattern is governed by the differential equation

$$\frac{\mathrm{d}}{\mathrm{d}t}C_l = R_{\mathrm{tot}}\left[C_l\eta\left(ld\frac{L-|vt-L|}{L_{\mathrm{T}}}\right)-C_l\right] \quad (8)$$

It describes how the final interferogram is blurred as the time interval of emission increases. Equation (2) follows then immediately after taking into account the time dependence of the emission rate due to cooling (equation (1)) and the fact that for our grating geometry, with a slit width of 470 nm and grating constant of 990 nm, only the lowest-order Fourier components contribute to the fringe visibility[30] $V = 2|C_1/C_0|$.

Received 15 September; accepted 8 December 2003; doi:10.1038/nature02276.

1. Joos, E. *et al. Decoherence and the Appearance of a Classical World in Quantum Theory* (Springer, Heidelberg, 2003).
2. Blanchard, P., Giulini, D., Joos, E., Kiefer, C. & Stamatescu, I.-O. (eds) *Decoherence: Theoretical, Experimental, and Conceptual Problems* (Lecture Notes in Physics 538, Springer, Heidelberg, 2000).
3. Imry, Y. *Introduction to Mesoscopic Physics*, 2nd edn (Oxford Univ. Press, Oxford, 2000).
4. Zurek, W. H. Decoherence, einselection, and the quantum origins of the classical. *Rev. Mod. Phys.* **75,** 715–775 (2003).
5. Pfau, T., Spälter, S., Kurtsiefer, Ch., Ekstrom, C. R. & Mlynek, J. Loss of spatial coherence by a single spontaneous emission. *Phys. Rev. Lett.* **73,** 1223–1226 (1994).
6. Chapman, M. S. *et al.* Photon scattering from atoms in an atom interferometer: coherence lost and regained. *Phys. Rev. Lett.* **75,** 3783–3787 (1995).
7. Kokorowski, D. A., Cronin, A. D., Roberts, T. D. & Pritchard, D. E. From single- to multiple-photon decoherence in an atom interferometer. *Phys. Rev. Lett.* **86,** 2191–2194 (2001).
8. Hornberger, K. *et al.* Collisional decoherence observed in matter wave interferometry. *Phys. Rev. Lett.* **90,** 160401 (2003).
9. Brune, M. *et al.* Observing the progressive decoherence of the "meter" in a quantum measurement. *Phys. Rev. Lett.* **77,** 4887–4890 (1996).
10. Myatt, C. J. *et al.* Decoherence of quantum superpositions through coupling to engineered reservoirs. *Nature* **403,** 269–273 (2000).
11. Buks, E., Schuster, R., Heiblum, M., Mahalu, D. & Umansky, V. Dephasing in electron interference by a 'which-path' detector. *Nature* **391,** 871–874 (1998).
12. Ji, Y. *et al.* An electronic Mach–Zehnder interferometer. *Nature* **422,** 415–418 (2003).
13. Arndt, M. *et al.* Wave–particle duality of C_{60} molecules. *Nature* **401,** 680–682 (1999).
14. Brezger, B. *et al.* Matter-wave interferometer for large molecules. *Phys. Rev. Lett.* **88,** 100404 (2002).
15. Patorski, K. in *Progress in Optics XXVII* (ed. Wolf, E.) 2–108 (Elsevier Science, Amsterdam, 1989).
16. Clauser, J. F. & Li, S. Talbot-von Lau atom interferometry with cold slow potassium. *Phys. Rev. A* **49,** R2213–R2217 (1994).
17. Dresselhaus, M. S., Dresselhaus, G. & Eklund, P. C. *Science of Fullerenes and Carbon Nanotubes* (Academic, San Diego, 1996).
18. Mitzner, R. & Campbell, E. E. B. Optical emission studies of laser desorbed C_{60}. *J. Chem. Phys.* **103,** 2445–2453 (1995).
19. Ding, D., Huang, J., Compton, R. N., Klots, C. E. & Haufler, R. E. Cw laser ionization of C_{60} and C_{70}. *Phys. Rev. Lett.* **73,** 1084–1087 (1994).
20. Hansen, K. & Echt, O. Thermionic emission and fragmentation of C_{60}. *Phys. Rev. E* **78,** 2337–2340 (1997).
21. Kolodney, E., Tsipinyuk, B. & Budrevich, A. The thermal energy dependence (10–20 eV) of electron impact induced fragmentation of C_{60} in molecular beams: experiment and model calculations. *J. Chem. Phys.* **102,** 9263–9275 (1995).
22. Matt, S. *et al.* Kinetic energy release distribution and evaporation energies for metastable fullerene ions. *Chem. Phys. Lett.* **303,** 379–386 (1999).
23. Nairz, O., Arndt, M. & Zeilinger, A. Experimental challenges in fullerene interferometry. *J. Mod. Opt.* **47,** 2811–2821 (2001).
24. Heszler, P., Carlsson, J. O. & Demirev, P. Photon emission from gas phase fullerenes excited by 193 nm laser radiation. *Chem. Phys.* **107,** 10440–10445 (1997).
25. Coheur, P. F., Carleer, M. & Colin, R. The absorption cross sections of C_{60} and C_{70} in the visible-UV region. *J. Phys. B* **29,** 4987–4995 (1996).
26. Hansen, K. & Campbell, E. E. B. Thermal radiation from small particles. *Phys. Rev. E* **58,** 5477–5482 (1998).
27. Hackermüller, L. *et al.* Wave nature of biomolecules and fluorofullerenes. *Phys. Rev. Lett.* **91,** 090408 (2003).
28. Clauser, J. F. in *Experimental Metaphysics* (eds Cohen, R. S., Home, M. & Stachel, J.) 1–11 (Kluwer Academic, Dordrecht, 1997).
29. Joos, E. & Zeh, H. D. The emergence of classical properties through interaction with the environment. *Z. Phys. B* **59,** 223–243 (1985).
30. Brezger, B., Arndt, M. & Zeilinger, A. Concepts for near-field interferometers with large molecules. *J. Opt. B* **5,** 82–89 (2003).

Acknowledgements We thank S. Uttenthaler for his support in an early stage of the experiment. We acknowledge support by the Austrian START programme, the Austrian FWF, the European TMR and Marie Curie programmes, and the DFG Emmy-Noether programme.

Authors' contributions L.H. performed most of the experiments as a part of her Ph.D. thesis. K.H. developed the decoherence theory, and made the quantitative comparison between experiment and theory.

Competing interests statement The authors declare that they have no competing financial interests.

Correspondence and requests for materials should be addressed to M.A. (markus.arndt@univie.ac.at).

High-transition-temperature superconductivity in the absence of the magnetic-resonance mode

J. Hwang[1], T. Timusk[1] & G. D. Gu[2]

[1]*Department of Physics and Astronomy, McMaster University, Hamilton, Ontario L8S 4M1, Canada*
[2]*Department of Physics, Brookhaven National Laboratory, Upton, New York 11973-5000, USA*

The fundamental mechanism that gives rise to high-transition-temperature (high-T_c) superconductivity in the copper oxide materials has been debated since the discovery of the phenomenon. Recent work has focused on a sharp 'kink' in the kinetic energy spectra of the electrons as a possible signature of the force that creates the superconducting state[1–14]. The kink has been related to a magnetic resonance[13,15–17] and also to phonons[18]. Here we report that infrared spectra of $Bi_2Sr_2CaCu_2O_{8+\delta}$ (Bi-2212), shows that this sharp feature can be separated from a broad background and, interestingly, weakens with doping before disappearing completely at a critical doping level of 0.23 holes per copper atom. Superconductivity is still strong in terms of the transition temperature at this doping ($T_c \approx 55$ K), so our results rule out both the magnetic resonance peak and phonons as the principal cause of high-T_c superconductivity. The broad background, on the other hand, is a universal property of the copper–oxygen plane and provides a good candidate signature of the 'glue' that binds the electrons.

We investigated the Bi-2212 material systematically as a function of doping, including highly overdoped Bi-2212 (see Methods). To better display the sharp 'kink', we do not show the optical conductivity but focus our attention on a related quantity, the optical single-particle self-energy, $\Sigma^{\mathrm{op}}(\omega)$ (see Methods). In Fig. 1a–d we plot the imaginary part of this quantity, which is simply the scattering rate of the charge carriers. At high frequencies the scattering rate varies linearly with frequency: this is called the marginal Fermi-liquid (MFL) behaviour[19]. We note that the overall scattering rate decreases as the doping increases and that there is a sharp depression in $1/\tau(\omega)$ below 700 cm^{-1} at low temperatures, with an overshoot in the superconducting state. This sharp onset of scattering has been in general attributed to the interaction of the charge carriers with a bosonic mode and more recently to the 41-meV neutron resonance[7,13,14]. In the real part of the optical self-energy, plotted in Fig. 1e–h, we note a sharp peak around 700 cm^{-1}, which tracks the depressions in $1/\tau(\omega)$ in both frequency and amplitude. One interesting property of the peak in the self-energy is its doping and temperature dependence: the peak gets weaker as the doping level and the temperature increase. We call the peak the 'optical resonance mode'. The resonance peak in the self-energy spectrum can clearly be resolved from the broader background of MFL scattering.

The optical self-energy is closely related to the quasiparticle self-energy $\Sigma^{\mathrm{qp}}(\omega)$, which can be measured in ARPES experiments although there are important differences in the two quantities[20–22]. In Fig. 2 we show a comparison of the optical self-energy from our data and the ARPES self-energy at two temperatures: one in the normal state and the other in the superconducting state. We see that although the qualitative features are very similar, the magnitudes and the frequency values of the various features differ considerably, as expected from theory. Part of the difference can be attributed to the uncertainty in locating the unrenormalized baseline in the ARPES analysis. As noted in ref. 6, a peak in $\Sigma_1^{\mathrm{qp}}(\omega)$ can be clearly separated from the broad continuum and is closely correlated with